Effect of Sandblasting, Etching and Resin bonding on the Flexural Strength/Bonding of Novel Glass-Ceramics

Chinwe O. Uwalaka [a], Natalia Karpukhina [a], Xu Cao [a], Sami Bissasu [a], Rory M. Wilson [b], Michael J. Cattell*[a]

[a] Centre for Oral Bioengineering, Bart's and the London, School of Medicine and Dentistry, Queen Mary University of London, Turner Street, Whitechapel, E1 2AD, UK. [b] School of Engineering and Materials Science, Queen Mary University of London, London, Mile End Road, E1 4NS, UK.

*corresponding author; email address: m.cattell@qmul.ac.uk

Abstract

Objectives: To process novel leucite glass-ceramics and test the effects of surface treatment and resin bonding on the biaxial flexural strength (BFS) and shear bond strength (SBS).

Methods: Alumino-silicate glasses were ball-milled, and heat treated to form leucite glass-ceramics (LG-C, OLG-C), then sintered into ingots. Ingots were heat extruded into a refractory mould to form disc specimens (1.3 x 14 mm diameter). IPS e.max® was used as a commercial comparison. Glass-ceramic test groups were sandblasted (Groups. 1, 4, 6) sandblasted, etched and adhesively bonded (Groups. 2, 5, 7) or lapped, etched and adhesively bonded (Groups. 3, 8). Specimens were adhesively bonded with Monobond S, followed by the application of Variolink II® cement and light curing. BFS testing was at 1mm/min and SBS testing at 0.5mm/min. Samples were characterised using XRD SEM and profilometry.

Results: XRD confirmed tetragonal leucite in LG-C/OLG-C and lithium disilicate/lithium orthophosphate in IPS e.max®. Mean BFS (MPa (SD)) were: Gp1 LG-C; 193.1 (13.9), Gp2 LG-C; 217.7 (23.0), Gp3 LG-C; 273.6 (26.7), Gp4 OLG-C; 255.9 (31); Gp5 OLG-C; 288.6 (37.4), Gp6 IPS e.max®; 258.6 (20.7), Gp7 IPS e.max®; 322.3 (23.4) and Gp8 IPS e.max®; 416.4 (52.6). The Median SBS (MPa) were Gp1 LG-C; 14.2, Gp2 LG-C (10 s etch); 10.6 and Gp3 IPS e.max®; 10.8. Mean surface roughness was 5-5.1 μm (IPS e.max®) and 2.6 μm (LG-C).

Significance: Novel leucite glass-ceramics with reduced flaw size and fine microstructures produced enhanced BFS and SBS by resin bonding. These properties may be useful for the fabrication of minimally invasive aesthetic and fracture resistant restorations.

Key Words: Glass-ceramic, X-ray Diffraction, Sandblasting, Acid-etching, Tetragonal Leucite.

1. Introduction

Leucite ($KAlSi_2O_6$) glass-ceramics are desirable for the fabrication of dental restorations due to their excellent aesthetic properties, which simulate natural tooth appearance and their low cytotoxicity [1]. The high thermal expansion coefficient of tetragonal leucite (20.5 x 10^{-6} / °C) [2], makes it a useful component in veneering materials for high strength metal-ceramic restorations [3]. Leucite glass-ceramics can also be fabricated into a variety of all-ceramic restorations adhesively bonded to dentine–enamel tooth structure [4, 5], and encouraging a more conservative tooth preparation [6]. Restorations can be processed by heat extruding glass-ceramic ingots into a refractory mould prepared by the lost wax technique, then finished by extrinsically staining to simulate the natural characteristics of the tooth [7]. Heat extrusion increases densification and is associated with higher flexural strength due to crystallite dispersion and a more homogeneous crystal distribution [8, 9]. Typical properties are a reported K_{IC} of 1.33 (0.08) MPa $m^{1/2}$ and flexural strengths in the range of 75.7–165 MPa [10, 11]. Mackert et al. [12] suggested that inherent flaws associated with the cubic to tetragonal transformation were reduced by synthesizing crystals in a critical size range (<4 μm). The synthesis and heat extrusion of a fine grained (<4um) leucite glass-ceramic resulted in a high flexural strength of (mean (SD)) 245 (24.3) MPa and high reliability (weibull m =11.9) [13]. Heat extrusion and processing including sandblasting and finishing are however, associated with a range of critical flaws, which when under tensile stress cause premature failure by various failure modes, initiated at occlusal contacts or cementation surfaces [14]. Resin bonding of leucite glass-ceramic restorations is advantageous in this respect as they are significantly strengthened by this modification to their internal surfaces

[15]. Internal ceramic surfaces can be sandblasted and etched to gain micromechanical retention, followed by silane bonding agents wetting and bonding to the ceramic surface. The organo-functional group in the silane next forms a bond with the resin cement [16, 17]. Effective resin-ceramic bonding of glass-ceramic restorations takes advantage of increased surface area for bonding to tooth structure to gain retention [15, 18] and reinforcement [5], and a clinically acceptable marginal fit [19, 20]. There is also the advantage of significant strengthening effects related to resin elastic modulus and thickness [21, 22]. Some pre-resin bonding surface treatments such as sandblasting, in addition to improving micro roughness, can change critical flaw populations and degrade strength [23]. Hydrofluoric (HF) acid etching has also been found to reduce the biaxial flexural strength of leucite glass-ceramics [24], and the type of silane employed can influence bond strengths [25]. When developing new glass-ceramic formulations the glass/ crystal phase chemistry, leucite crystal size, number and distribution [15], and physical properties influence the resultant bonding surface area and structure after pre-cementation treatments. The subsequent micromechanical retention and wettability of these surfaces is important to achieve effective adhesive resin bonding [26]. The authors have synthesised a unique range of new leucite glass-ceramics with high leucite volume fraction and small crystallite size for the first time [27]. It is therefore key to asses these ceramics after scale-up and following processing and cementation procedures, to realise the optimisation of this important category of materials and its benefits for minimally invasive adhesive dentistry. Therefore, the aims of this study were to process novel leucite glass-ceramics (LG-C, OLG-C) using heat extrusion and to analyse the effects of sandblasting, etching and resin bonding on the biaxial flexural strength and the shear bond strength of the glass-ceramics.

2. Materials and Methods

2.1 Preparation of Sandblasted Specimens

An alumino-silicate glass with the following composition (mol %) was commercially synthesized (Lot nos: F-0356, 92100111, glasses supplied by Davis Schottlander Davis Ltd., UK and Cera Dynamics Ltd, Stoke-on-Trent, UK): SiO_2 (69.7 %), Al_2O_3 (10.6 %), K_2O (12.8 %), CaO (1.5 %), TiO_2 (1.3 %), Na_2O (1.9 %), Li_2O (1.6 %), B_2O_3 (0.7 %) by heating in a high temperature custom made furnace (Cera Dynamics Ltd, UK) at 10°C/min to 1550°C (5 h hold). The glass was air quenched and allowed to cool to room temperature. The glass frit was crushed, ball-milled for 1 h and screened to 125 µm (LG-C). To optimise the glass-ceramics another batch of glass was also produced using the same parameters but quenched in water and ball milled for 93 h, followed by spray drying (Niro Atomizer, Denmark) of the powder (OLG-C).

The glass powders (LG-C and OLG-C) were placed into refractory trays (IPS press Vest speed, Ivoclar-Vivadent, Lot no: Powder TL3033 and Liquid TL3022) and heated in a furnace (Lenton 1600, Hope Valley, UK) at 10°C/ min to 592 °C (1h hold), then ramped at 10°C/min to 1040°C (30 min hold). The leucite glass-ceramic (LG-C) and optimised leucite glass-ceramic (OLG-C) were air quenched, ball-milled and screened through a 125 µm sieve (Endescott Ltd, London, UK). To fabricate glass-ceramic ingots 1.6 g of LG-C or OLG-C powder was dry compacted using a custom-made steel die and punch (diameter 13.0 mm, Specac Ltd., Slough, UK), by applying 0.5 bar pressure for 30 s using a hydraulic press (Quayle Dental, HBP 153, UK). Compacted powder ingots were ramped from 538°C at a rate of 38°C to 1060°C, under partial vacuum (55 hPa) and held for 2 min in a porcelain furnace (Multimat 2 Touch + Press, Dentsply, Weybridge, UK).

IPS e.max® (LT A3, Ivoclar-Vivadent, Lot no: T45580) was used as a commercial comparison. Perspex (ICI Plastics, UK) discs (1.3 mm depth x 14 mm diameter) were sprued onto muffle bases with a surrounding silicon cylinder. Disc specimens were invested using 200 g of investment material (IPS Press VEST speed powder, Lot no: TL3033), mixed with 32 ml liquid (Lot no: TL3022) and 22 ml distilled water and vacuum mixed (Renfert twister; E10022C6, Germany) at 350 rpm for 2.30 min. The investment was poured into the moulds under vibration and allowed to set for 45 min, then placed into a furnace (Renfert Magma, B1099520, Germany) preheated to 850°C and allowed to dwell for 60 min. The LG-C, OLG-C or IPS e.max® ingots (at room temperature) were placed into hot refractory moulds, then heat pressed using a press furnace (Programat EP 3000, Ivoclar-Vivadent, Schaan Liechtenstein) according to the protocols in Table 1. LG-C, OLG-C and IPS e.max® specimens were divested via a sandblasting unit (Renfert Basic Quattro, Germany) using 50 μm glass beads (07M509B, Bracon Ltd, UK) at 2 bar pressure. The sandblasting nozzle was held at 10 mm from specimen's surface and at 45° to the specimens. Sprue areas were cut off using a diamond disc (006 Bracon Ltd., UK) and diamond bur (9907, Bracon Ltd., UK). Following divesting, LG-C and OLG-C discs were ultrasonically cleaned using distilled water in an ultrasonic bath (Sonorex RK 100H, Bandelin, Germany) for 10 min and air dried for 30 min. IPS e.max® G-C specimens following divesting had the reaction layers removed by immersion into invex liquid (lot no: H31070, Ivoclar-Vivadent AG, Germany) for 20 min. The residual acid solution was rinsed off the specimen under running water for 30 min, followed by sandblasting with 100 μm Al_2O_3 (lot no: 1644568, Renfert, Germany) using the same regimen as with the glass beads. Specimens were ultrasonically cleaned in distilled water (10 min) and air dried as previously.

2.2 Preparation of the Resin-bonded Specimens for the BFS Tests

The LG-C and OLG-C disc specimens (1.3 x 14 mm) prepared in 2.1 were split into 4 groups (n= 20 per group). Group 1 and 4 were tested as sandblasted. Group 2 and group 5 were sandblasted and resin bonded. Prior to resin bonding, the tensile surfaces were etched for 60 s (80 s for OLG-C) with 5 % Hydrofluoric (HF) acid (IPS ceramic etching gel, Lot no: T31384, Ivoclar-Vivadent) then rinsed under running water for 2 min. One measuring spoonful of IPS neutralising powder (lot no: T34017, Ivoclar-Vivadent) was spread over the etched surface for 5 min, rinsed under running water for 1 min then ultrasonically cleaned in distilled water for 3 min and air dried (30 min). Monobond S (lot no T29123, Ivoclar-Vivadent AG, Germany) was applied on the etched surfaces of the LG-C and OLG-C specimens and allowed to air dry for 60 s. Variolink II Base (lot no: T30272, Ivoclar-Vivadent) and Catalyst (lot no: T00901) were mixed for 10 s at a ratio of 1:1 and applied to the prepared surfaces. A mylar strip was placed over the resin followed by a glass cover slip and a 50 N weight for 1 min. The resin was light cured using an LED dental curing light (Bluephase16i, Ivoclar-Vivadent) at the SOF setting, placed at a distance of 1 mm over the centre of the specimen and cured for 15 s, then at three different points on the disc circumference for 10 s. Group 3 was sandblasted, lapped to P800 grit silicon carbide paper (Buehler, Coventry UK), then etched, neutralised and resin bonded as in Group 2.

IPS e.max® G-C disc specimens prepared in 2.1 were split into three groups (n= 20 per group). Group 6 was as sandblasted with 100 μm Al_2O_3 as described in 2.1. Group 7 was HF etched for 20s, neutralised and resin bonded as previously. Group

7 was lapped to P800 grit silicon carbide paper, and then HF etched for 20s, neutralised and resin bonded using the earlier protocol. The prepared LG-C, OLG-C and IPS e.max® specimens were stored at 37°C for 24 h in an incubator (Camlab, UK) prior to mechanical testing. Test groups are illustrated in Table 2.

2.3. Preparation of the Resin-bonded Specimens for the SBS Tests

LG-C and IPS e.max® G-C disc specimens as sandblasted in 2.1 were ultrasonically cleaned in distilled water and divided into three groups (n= 10 per group). Group 1 (LG-C) was etched using 5% HF acid (IPS ceramic etching gel, Ivoclar-Vivadent, Lot no: T31384) for 60 s and Group 2 (LG-C) etched for 10 s, while Group 3 (IPS e.max®) was etched for 20 s. The rinsing, neutralisation, cleaning and monobond S application procedures were identical to 2.2. During resin application, Tygon tubing (5 mm diameter x 2 mm depth, R3603, Norton Performance Plastic Corp, USA) was centrally positioned on the specimen surface and Variolink II® resin cement (prepared as previously) placed into the tubing at 1 mm increments. Each 1 mm increment was light cured centrally for 15 s and at three different points around the circumference for 10 s each, using an LED dental curing light (Bluephase16i, Ivoclar-Vivadent) on the SOF setting. Following light curing, the LG-C and IPS e.max® G-C specimens were stored in distilled water at 37°C for 7 days before SBS testing.

2.3 Biaxial Flexural Strength Testing

The biaxial flexural strength (BFS) of glass-ceramic groups shown in Table 2 were tested using the ball-on-ring test. Disc specimens were placed on a 10 mm diameter knife-edge support and centrally loaded via a 4 mm diameter spherical ball indenter at a crosshead speed of 1 mm/min until specimen failure. The BFS of the as sandblasted Groups 1, 4 and 6 were calculated using the Timoshenko and Woinowsky-Krieger equation [28]:

$$\sigma_{max} = P/h^2 \{(1+v)[0.485x\ln(\alpha/h)+0.52]+0.48\}$$

where σ_{max} was the maximum tensile stress, P was the load at fracture, h was the thickness of the specimen, a was the radius of knife-edge ring support, v was the Poisson's ratio of 0.25 [29].

The maximum tensile stress (σ), of the resin-bonded groups (Table 2), were calculated using a multi-layer equation, described by Hsueh et al. [30]. Values for modulus of elasticity and Poisson's ratio for the respective glass-ceramics and resin cement were entered into the equation. The modulus of elasticity values for the leucite glass-ceramics (LG-C/OLG-C) were taken to be 65 GPa [31] and 95 GPa [32] for IPS e.max® glass-ceramic. The Poisson's ratio of the glass-ceramics was taken to be 0.25 [29] and for the resin cement was 0.33 [33]. The modulus of elasticity of the resin cement and taken to be 7.6 GPa [33].

2.4 Statistical Analysis

One-way ANOVA (Sigma Stat, version 2.03, SPSS Inc., Chicago, USA) and Tukey's multiple comparison tests ($p < 0.05$) was used to compare the BFS test groups. The biaxial flexure strength data were ranked in ascending order and the Weibull analysis using Weibullsmith software (Fulton Findings, USA) was performed. The double logarithm of 1/ (1-median rank) was plotted vertically against the logarithm of the actual data values and a straight line fitted through the points using the median rank regression methods. The equation of Weibull two parameter distribution function used was:

$$P_f = 1 - \exp[-(\frac{\sigma}{\sigma_0})^m]$$

Where P_f is the probability of failure and (σ) is the strength at a given P_f value. σ_0 is the characteristic strength and m is the Weibull modulus. Groups were compared according to the overlap of their double-sided confidence intervals at the 95% level.

2.5. Shear Bond Strength Test

10 specimens per test group, LG-C (10 and 60s etch) and IPS e.max® (20s etch), were loaded in a universal testing machine (Instron 5567, Instron Ltd., UK), using a knife edge chisel placed perpendicular to the resin-ceramic interfaces at a crosshead speed of 0.5mm/min until failure. The shear bond strength (SBS) was calculated using the equation:

$$SBS = \frac{F}{\pi r^2}$$

Where F is the maximum force (N) and r is the radius of the composite cylinder. Data sets were compared using the Mann-Whitney rank sum test.

2.6 Secondary Electron Imaging (SEI)

Glass-ceramic specimens were polished to 1µm alumina micropolish (Lot no: 0335-0275, Buehler, Coventry, UK) and etched (LG-C/OLG-C; 0.1% HF, 60 s) and for IPS e.max® (2% HF mixed with 15% sulphuric acid, 10 s). Polished and fractured specimens were gold coated in an automatic sputter coater (Agar Scientific Ltd., UK) for 30 s at 40 mA and viewed using a field emission scanning electron microscope (FEI Inspect F, Eindhoven, The Netherlands) in the secondary electron imaging mode.

2.7. X-ray Diffraction Analysis

LG-C, OLG-C and IPS e.max® G-C powders were analysed using a Panalytical X'Pert Pro powder diffractometer (Panalytical B.V., Almelo, The Netherlands). CuKα radiation was used with the tube powered at 45 kV and 40 mA. Data was collected continuously with an X'Celerator solid state multistrip detector from 5° to 70° (2 ϴ range) with a step size of 0.0334° and a step time of 200.03 s. Calibration was carried out using NIST standard reference material 660 a (lanthanum hexaboride). Crystal phases were identified using ICDD reference codes 00-038-1423 for tetragonal leucite, 40-0376 for Lithium disilicate and 01-087-0039 for β-lithium orthophosphate.

2.8 Profilometry Analysis

The surface roughness for the heat pressed and sandblasted LG-C and IPS e.max® G-C disc specimens were analysed before and after etching using the non-contact 3D White-light profilometer (Proscan-2000, Scantron, Taunton, UK). A dark background measurement was carried out for the sensor before conducting any

scans to ensure that a maximum sensitivity to the reflected light was achieved. An S13/1.2 chromatic sensor was used (Stil S.A., Aix-enProvence, France) and samples were scanned at a frequency of 100 Hz using a step size of 5 μm and a surface area of (4 x 4 mm) that acquired profilometric surface image of 801 lines (x and y). All scanned data were analysed using the dedicated software (Proform ver. 1.41, Proscan-2000 ver. 2.1.8.8+ software, Scantron, UK) and a surface filter of 80 % was applied on all scanned images.

3. Results

3.1 Biaxial Flexural Strength Test Results

The biaxial flexural strength (BFS) results are presented in Table 3. There was a statistically significant difference ($p < 0.05$) between BFS groups 1 and 2, 4 and 5 and between 7 and 8. There was no significant difference ($p > 0.05$) between sandblasted OLG-C (group 4) and the IPS e.max® G-C (group 6) mean BFS values, however the LG-C (group 1) had a significantly lower mean BFS value. After resin bonding the IPS e.max® G-C (group 7 and 8) had a significantly higher (mean BFS value than the resin bonded OLG-C (group 5).

The results of the Weibull analysis are reported in Table 3. There was no significant difference in Weibull m values between groups 2, 3, 4, 5, 6 and 8. The group 1 m value was significantly higher than groups 4, 5 and 8. There were significant differences in characteristic strength between groups 1, 2, 3, 5, 6, 7 and 8. Group 4 was significantly different to all the other test groups apart from groups 3 and 6 characteristic strengths, according to the overlap of their 95% double sided confidence intervals.

3.2 Secondary Electron Imaging Results

SEI photomicrographs of LG-C, OLG-C and IPS e.max® G-C are presented in Figures 1a-h. The LG-C had a uniform dispersion of spherical leucite crystals with a mean (SD) crystal size of 0.89 (1.08) μm^2 and the OLG-C a mean (SD) crystal size of 0.62 (0.42) μm^2.There was no microcracking in the glass matrix observed for LG-C (Fig. 1a) and OLG-C (Fig. 1b). IPS e.max® G-C showed the characteristic rod-like crystals of lithium-disilicate (Fig. 1f). LG-C illustrated fine trans-granular fracture

surfaces (Fig. 1d), in contrast with the coarser inter-granular fracture surface of the IPS e.max® (Figs 1f). Crack pinning and possible crack bridging mechanisms were visible in the LG-C fracture surface (Fig. 1e). LG-C and IPS e.max® G-C indicated fracture surfaces where failure was initiated at the ceramic-cement interface or near this interface (1g-h).

For the SBS specimens 100% of the LG-C specimens (10 and 60 s, HF etched) failed cohesively into the ceramic (Figs. 2a-b) and only 20% of IPS e.max® G-C (20 s HF etched) showed similar cohesive failure. The remaining 80% showed largely interfacial mixed mode failure (Figs. 2c-d).

3.3 Shear Bond Strength Test Results

The shear bond strength (SBS) test results are shown in Table 4. The LG-C (group 1) had a significantly higher ($p < 0.05$) mean and median SBS than IPS e.max® G-C (group 3). There was no significant difference ($p > 0.05$) in SBS values between groups 2 and 3. There was no significant difference ($p > 0.05$) in the median SBS between LG-C Groups 1 and 2.

3.4 X-ray Diffraction Results

X-ray diffraction results for the powdered LG-C and OLG-C specimens identified tetragonal leucite as the major crystal phase (Fig 3a). Lithium disilicate was the major phase and β-lithium orthophosphate a minor phase in the IPS e.max® G-C (Fig 3b).

3.5. Profilometry Results

The surface roughness values for sandblasted LG-C and IPS e.max® G-C, before and after acid etching are given in Table 5. Profilometric image of the LG-C and IPS e.max® G-C after sandblasting and acid etching are shown in Figs 4a, b. The recorded roughness values (R_a) for the LG-C disc sample were lower than the IPS e.max® G-C. The R_a in both samples was consistent across the X and Y directions, which illustrates that the flaw sizes in the LG-C and IPS e.max® G-C were uniformly distributed. After acid etching the glass-ceramic samples, a decrease in the surface roughness (R_a) from 3.1 to 2.6 μm for LG-C and from 5.7 to 5 μm for IPS e.max® G-C was achieved.

4. Discussion

Tetragonal leucite was confirmed by X-ray diffraction to be the major crystalline phase in the experimental leucite glass-ceramics (OLG-C, LG-C) (Fig. 3a). Leucite crystal twinning, characteristic of the tetragonal leucite phase was also observed in the SEM photomicrographs (Fig 1a-b). Lamellar and merohedric twinning has been described by Palmer et al. [34] and is a consequence of complex stresses induced by the reversible cubic to tetragonal phase transformation of leucite crystals cooling from above 400°C to 25°C. This phenomenon is accompanied by a reversible 1.2% change in volume of the unit cell which induces tangential stresses around the crystals and its surrounding glassy matrix. Tetragonal leucite reinforced glass-ceramics are strengthened by these complex induced stresses [34, 35]. The LG-C and OLG-C featured a high area fraction (56.6% and 69%, respectively) of well bonded tetragonal leucite crystals, homogeneously dispersed within the microcrack-free glassy matrix (Figs. 1a-b). The relationship between leucite crystal growth and the remaining potassium deficient residual glass and its subsequent thermal expansion, was suggested as responsible for increased fracture strength [36]. The LG-C featured a higher BFS (mean (SD) =193.1 MPa (13.9)) than the strength range reported (75.7–165 MPa) for leucite glass-ceramics [10, 11]. Optimisation of the powder processing and spray drying of the glass powder took advantage of surface crystallisation effects discussed previously [11]. A reduction in the crystal size from 0.89 to 0.62 μm^2 was gained in the OLG-C Group which drove up the flexural strength by 32.5% to 255.9 (31.0) MPa. The absence of micro-cracks in the glass matrix (Fig. 1b) indicates a favourable CTE match between the crystal and matrix phases [37], and that crystal sizes were in the critical (<4μm) range for limiting microcracking [12]. Flaws in leucite reinforced glass-ceramics are thought to

propagate through both the crystals and the glassy matrix via a trans-granular mechanism [38]. A homogeneous dispersion of fine crystals within the matrix created a fine fracture surface (Fig. 1d). It appeared there was a more complex pattern of crack propagation and increased potentials for micro-crack bridging, pinning (Fig. 1e) and other crack deflection mechanisms [38, 39].

XRD of IPS e.max® G-C confirmed the major and minor crystal phases to be $Li_2Si_2O_5$ and Li_3PO_4 respectively (Fig 3b). The high-volume fraction (70 ± 5 vol.% [10]) of lithium disilicate fibres found in the IPS e.max® G-C (Fig 1c) are reported to resist crack propagation by means of their high aspect ratio fibres. The intergranular fracture process [38] can be seen in the rough fracture surface (Fig. 1f), resulting in high fracture toughness (3.3 ± 0.3 $MPa.M^{0.5}$) [40]. The Mean (SD) BFS of sandblasted IPS e.max® G-C in this study (258.6 (20.7) MPa) was less than the manufacturers values (300-400 MPa) [32], or higher reported values (440 (55.0) MPa) [31] for lapped and fired /annealed specimens. The Flexural strength was however, recovered in the group 8 IPS e.max® specimens (416.4 (52.6) MPa) when the flaw population was modified by lapping and adhesive bonding (Table 2). It was therefore thought that the reduced BFS of the group 6 specimens (sandblasted IPS e.max®) was associated with processing induced surface flaws cited in the literature [41, 42]. Profilometry of the surface following treatment with invex acid and sandblasting (100 μm Al_2O_3) regimens (as recommended by the manufacturers) produced a surface roughness (R_a) value of 5.7μm reduced to 5.0 μm after 20 sec hydrofluoric acid (HF) etching (Fig. 5b, Table 5). These flaws can act as stress concentrators causing cracks to propagate at a lower applied force [23, 43]. Sandblasting creates micromechanical retention for bonding but reduced flexural strengths in lithium disilicate glass-ceramic specimens (IPS e.max® CAD, Ivoclar-

vivadent), when abraded with 30 μm Al_2O_3 media (100-300 KPa pressure) [44]. In the current work, the increased erosion rate and subsequent surface roughness may be related to the square of the grit diameter [43], since 100 μm Al_2O_3 (150 KPa pressure) was used. Surface damage following sandblasting is however multifactorial and determined by the hardness, impact velocity, angle of impact and morphology of the blasting material [23, 43], as well as the physical properties of the glass-ceramic substrate. The use of Invex acid (0.6% HF and 1.7% sulfuric acid (Ivoclar-Vivadent) prior to sandblasting was to ensure the removal of any reaction layer with the investment. Vidotti et al. [45] indicated that after 20 min invex acid exposure there was no significant morphological surface changes, or differences in bond strengths for lithium disilicate glass-ceramics (IPS e.max® Press) compared to untreated controls. The sandblasting regimen in group 6 specimens may therefore be the major controlling factor influencing strength values. Alumina particle air abrasion (25-110 μm Al_2O_3) of feldspathic porcelains led to weakening of these materials, with a reduction in reliability for 110 μm Al_2O_3 abraded specimens, potentially associated with subsurface damage and flaw instability [23]. The extent of surface damage caused by the processing procedures on the IPS e.max® G-C was evident as it possessed almost twice the mean R_a value of the LG-C (Tables 5, Figs 5a-b). Since all sandblasting variables were kept constant the media size, morphology, chemical composition/hardness and the properties of the substrates effected the mean R_a values. The sandblasted (50 μm glass beads) LG-C exhibited a lower BFS compared to IPS e.max® G-C (100 μm Al_2O_3). The 50 μm glass blasting media created a different flaw size distribution in conjunction with the LG-C substrate (Fig 5a). The complexities of particle shape, size and erosion efficiency is discussed elsewhere [24], with sharp angular particles producing ploughing and cutting effects

at low angles [43]. Optimisation of the glass-ceramic microstructure (OLG-C, group 4) in conjunction with the 50 μm glass bead sandblasting process resulted in increased mean (SD) BFS (255.9 (31.0) MPa) and characteristic strength, with no statistical difference with the sandblasted IPS e.max® G-C (group 6, Table 3).

The mean R_a values of both the IPS e.max® G-C and LG-C reduced by 12.2% and 16.1% respectively following HF acid etching (20 and 60 secs, Table 5, Figs 4a-b). This 5% HF treatment and durations used reduced the surface flaw sizes on both materials, which may have reduced the severity of surface defects. HF etching (20 secs) of lapped IPS e.max® G-C resulted in no significant flexural strength reduction, but with resin infiltration the flexural strengths increased to mean (SD) 420 (31) MPa, [46], in agreement with the current lapped values of 416.4 (52.6) MPa (Table 3). The reduced glassy phase available for etching lithium disilicate materials [46], or preferential etching of the leucite crystalline phase may be factors, as feldspathic porcelains indicated increased ceramic roughness (mean R_a) and reduced BFS on HF addition [47]. HF Etching of ceramic materials with different glass-crystal chemistry and crystalline morphology will result in differing surface roughness, morphology, pore structure and wettability [48]. This was reflected in the SBS study with interfacial mixed mode failure (Figs. 2c-d) and lower bond strengths for the IPS e.max® G-C associated with the larger flaw size distribution or efficacy of etching (5% HF) the glassy phase at 20 secs. Etching (10 and 60 secs) of the leucite crystallites [17] in LG-C should produce a different surface area, morphology of etching and smaller flaw size which resulted in 100% cohesive failure in the ceramic (Figs 1a-b). Interestingly, fatigue and fracture testing of IPS e.max® Press laminate veneers adhesively bonded to human central incisors resulted in >50% adhesive

failures (between resin cement and glass-ceramic), suggesting adhesion improvements were possible [49].

All glass-ceramic (LG-C, OLG-C and IPS e.max® G-C) groups had a significant increase in BFS (12.7-24.6%, Table 3) and characteristic strength following acid etching and adhesively bonding via a silane bonding agent and resin cementation. This was not surprising since adhesive bonding has been found to strengthen dental ceramic materials [21, 22]. Previous strengthening theories suggest a combination of flaw recovery [50], and the generation of compressive stresses due to polymerisation shrinkage [5]. This strengthening effect may however be attributed to the interpenetration of the resin into the ceramic surface creating a hybrid layer and sensitive to the resin modulus [21]. Fleming et al. [51] suggested a significant ceramic reinforcement using a resin coating of 50 μm, with the flexural modulus and resin thickness related to the degree of strengthening. Resin thickness for IPS e.max® and LG-C (groups 2 and 7) was 45 (20) μm and 50 (30) μm respectively which was in this resin-ceramic strengthening range. Increased resin flexural modulus (12.6 (0.4) GPa led to a 47% increase in ceramic BFS [51]. The flexural modulus of Variolink II resin used in this study was 5.0 (1.36) GPa [52], so there is a potential for a strength enhancement by optimising this property, but with ensuring sufficient wetting of the ceramic interface. The IPS e.max® G-C benefitted most from resin bonding with a significant increase in BFS (24.6%, Table 3). This was related to the interaction of the resin layer with the surface defect population (5-5.1 μm, Fig. 5b), and with the magnitude of resin strengthening sensitive to ceramic surface texture [53]. When the ceramic surface sandblasting flaws were removed by lapping (800 grit silicon carbide paper), followed by etching and resin addition there was a remarkable 61% increase in BFS (416.4 (52.6) MPa) when compared with the

sandblasted group 6 (258.6 (20.7) MPa). Other factors can be removal of any porosity or surface crystallisation that may differ from the interior and the generation of residual stresses [54]. A moderate BFS increase was also encountered for the LG-C on adhesive bonding and following lapping, etching and resin addition there was a 41% increase in BFS. The LG-C had a much smaller flaw size (2.6 μm, Table 3), and a different profilometric profile and flaw size distribution (Fig. 5a) compared to the IPS e.max® G-C. Optimisation of the microstructure (OLG-C, group 5) necessitated an increased etching time (80 sec) and following cement addition a significant increase in BFS (mean (SD) 288.6 (37.4) MPa) over the LG-C groups 1 and 2 ($p<0.05$). Etching of the glass-ceramic phases and the differing surface areas for micromechanical retention and wettability will affect resin penetration and reaction of the silane and resin composite [48]. The resin-ceramic interaction at the interface can therefore be easily modified by these numerous factors and the interplay with the very different fracture mechanisms present in these materials [39, 55]. The texture of the differing failed specimens illustrated these different fracture processes (Fig 1d-f). Fractographic analysis of the failed BFS specimens revealed fracture origins in the IPS e.max® G-C originated from the resin-ceramic interface (Fig. 1h), whereas the LG-C exhibited interfacial and interior flaw failure (Fig 1g).

Dental glass-ceramics are processed using CAD-CAM technology, heat extrusion or sintering and this results in processing flaws of differing severity and distribution. At present, lithium disilicate glass-ceramics require an additional crystallisation heat treatment after machining or removal of a reaction layer following heat extrusion. The developed leucite glass-ceramics (LG-C OLG-C) do not require these lengthy processes and there is potential to control the surface stress state and modify defects through extended glaze firing cycles [56], or ion exchange to further improve

strengthening [57]. This study highlights current heat extrusion processing defects and their subsequent effects on BFS and SBS. Similar flexural strengths were achieved for heat pressed lithium disilicate and leucite glass-ceramic sandblasted materials. Although the IPS e.max® G-C resulted in the highest mean (SD) BFS of 322.3 (23.4) MPa, following adhesive bonding the optimised leucite glass-ceramics produced a high mean (SD) BFS of 288.6 (37.4) MPa and with the possibility of further strength enhancements by resin cement developments. Their fine crystal size, uniform microstructure and smaller etched flaw size (2.6 μm) appears to provide sufficient bond strength and high flexural strength at 1 mm depth. This allows minimal tooth preparation, retention to tooth structure and avoids destructive tooth reduction needed for retentive preparations [58]. Previous work also indicates reduced enamel wear [59] with these high strength leucite glass-ceramics.

They possess some properties beneficial for adhesively bonded monolithic crowns or veneers to improve poor survival rates [60, 61]. The glass refractive index is also matched with the leucite crystal phase, to ensure translucency [27] and good aesthetics [27] to meet the patients expectations. This work has therefore opened the window to extend the clinical use of this important category of biocompatible glass-ceramic materials in minimally adhesive dentistry.

Acknowledgements

The Authors gratefully acknowledge funding and support for this project from Dr Brian Schottlander (Davis Schottlander Davis Ltd.). Cera Dynamics Ltd are thanked for work on the glass scale up. Dr Jamila Almuhamadi and Dr R. Bailey (School of Engineering and Materials Science, QMUL) are acknowledged for help with the SEM and profilometry. We would also like to thank Cara (the Council for At-Risk Academics) for support.

References

[1] Messer RL, Lockwood PE, Wataha JC, Lewis JB, Norris S, Bouillaguet S. In vitro cytotoxicity of traditional versus contemporary dental ceramics. J Prosthet Dent 2003;90:452-8.

[2] Mackert JR, Evans AL. Effect of cooling rate on leucite volume fraction in dental porcelains. J Dent Res 1991;70:137-9.

[3] Weinstein M, Katz S, Weinstein B. Fused porcelain-to-metal teeth. US Patent 3,052,982, 1962.

[4] Kramer N, Frankenberger R. Clinical performance of bonded leucite-reinforced glass ceramic inlays and onlays after eight years. Dent Mater 2005;21:262-71.

[5] Nathanson D. Principles of porcelain use as an inlay/onlay material. In: Garber DA, Goldstein RE, editors. Porcelain and composite inlays and onlays, esthetic posterior restorations. Carol Stream, IL. Quintessence; 1994. p. 32-6.

[6] Van Dijken JW, Hasselrot L. A prospective 15-year evaluation of extensive dentin-enamel-bonded pressed ceramic coverages. Dent Mater 2010;26:929-39.

[7] Wohlwend A, Schärer P. The Empress technique for the fabrication of full ceramic crowns inlays and veneers. Quintessenz Zahntech 1990;16:966-78.

[8] Cattell MJ, Chadwick TC, Knowles JC, Clarke RL, Lynch E. Flexural strength optimisation of a leucite reinforced glass ceramic. Dent Mater 2001;17:21-33.

[9] Dong JK, Luthy H, Wohlwend A, Schärer P. Heat-pressed ceramics: technology and strength. Int J Prosthodont 1992;5:9-16.

[10] Höland W, Rheinberger V, Schweiger M. Control of nucleation in glass ceramics. Philos T Roy Soc A 2003;361:575-88.

[11] Theocharopoulos A, Chen X, Wilson RM, Hill R, Cattell MJ. Crystallization of high-strength nano-scale leucite glass-ceramics. Dent Mater 2013;29:1149-57.

[12] Mackert JR, Twiggs SW, Russell CM, Williams AL. Evidence of a critical leucite particle size for microcracking in dental porcelains. J Dent Res 2001;80:1574-9.

[13] Chen X, Chadwick TC, Wilson RM, Hill RG, Cattell MJ. Crystallization and flexural strength optimization of fine-grained leucite glass-ceramics for dentistry. Dent Mater 2011;27:1153-61.

[14] Zhang Y, Sailer I, Lawn BR. Fatigue of dental ceramics. J Dent 2013;41:1135-47.

[15] Blatz MB, Sadan A, Kern M. Resin-ceramic bonding: a review of the literature. J Prosthet Dent 2003;89:268-74.

[16] Van Noort R. Introduction to dental materials. London. Mosby; 1994. p. 61-71.

[17] Stangel I, Nathanson D, Hsu CS. Shear strength of the composite bond to etched porcelain. J Dent Res 1987;66:1460-5.

[18] el-Mowafy O. The use of resin cements in restorative dentistry to overcome retention problems. J Can Dent Assoc 2001;67:97-102.

[19] Keshvad A, Hooshmand T, Asefzadeh F, Khalilinejad F, Alihemmati M, Van Noort R. Marginal gap, internal fit, and fracture load of leucite-reinforced ceramic inlays fabricated by CEREC inLab and hot-pressed techniques. J Prosthodont 2011;20:535-40.

[20] Guess PC, Vagkopoulou T, Zhang Y, Wolkewitz M, Strub JR. Marginal and internal fit of heat pressed versus CAD/CAM fabricated all-ceramic onlays after exposure to thermo-mechanical fatigue. J Dent 2014;42:199-209.

[21] Addison O, Marquis PM, Fleming GJ. Resin elasticity and the strengthening of all-ceramic restorations. J Dent Res 2007;86:519-23.

[22] Hooi P, Addison O, Fleming GJP. Quantifying ceramic resin strengthening by varying the resin elasticity. Dent Mater 2009;25:e5-e46.

[23] Addison O, Marquis PM, Fleming GJ. The impact of modifying alumina air abrasion parameters on the fracture strength of a porcelain laminate restorative material. Dent Mater 2007;23:1332-41.

[24] Hooshmand T, Parvizi S, Keshvad A. Effect of surface acid etching on the biaxial flexural strength of two hot-pressed glass ceramics. J Prosthodont 2008;17:415-9.

[25] Hooshmand T, Matinlinna JP, Keshvad A, Eskandarion S, Zamani F. Bond strength of a dental leucite-based glass ceramic to a resin cement using different silane coupling agents. J Mech Behav Biomed Mater 2013;17:327-32.

[26] Aboushelib M, Ghoniem M, Mirmohammadi H, Salameh Z. General principles for achieving adequate bond to all-ceramic restorations. J Dent Oral Hyg 2009;1:36-41.

[27] Theocharopoulos A, Chen X, Karpukhina N, Hill R, Cattell MJ. Leucite glass-ceramics. US Patent 9,856,165, 2018.

[28] Timoshenko SP, Woinowsky-Krieger S. Theory of plates and shells. 2nd ed. New York: McGraw-Hill; 1959. p. 70-1.

[29] Zeng K, Oden A, Rowcliffe D. Evaluation of mechanical properties of dental ceramic core materials in combination with porcelains. Int J Prosthodont 1998;11:183-9.

[30] Hsueh CH, Luttrell CR, Becher PF. Analyses of multilayered dental ceramics subjected to biaxial flexure tests. Dent Mater 2006;22:460-9.

[31] Albakry M, Guazzato M, Swain MV. Biaxial flexural strength, elastic moduli, and x-ray diffraction characterization of three pressable all-ceramic materials. J Prosthet Dent 2003;89:374-80.

[32] Bühler-Zemp. P, Völkel T, Fischer K. Scientific Documentation IPS e.max Press. Schaan, Liechtenstein: Ivoclar Vivadent; 2011. p. 1-40.

[33] Dong XD, Darvell BW. Stress distribution and failure mode of dental ceramic structures under Hertzian indentation. Dent Mater 2003;19:542-51.

[34] Palmer DC, Dove MT, Ibberson RM, Powell BM. Structural behavior, crystal chemistry, and phase transitions in substituted leucite: High-resolution neutron powder diffraction studies. Am Mineral 1997;82:16-29.

[35] Denry IL, Holloway JA, Colijn HO. Phase transformations in a leucite-reinforced pressable dental ceramic. J Biomed Mater Res 2001;54:351-9.

[36] Assmann S, Ermrich M, Kunzmann K. Determination of quantitative leucite content in pressable ceramics compared to conventional dental porcelains. J Mater Sci Mater Med 2000;11:833-5.

[37] Mackert JR, Butts MB, Fairhurst CW. The effect of the leucite transformation on dental porcelain expansion. Dent Mater 1986;2:32-6.

[38] Apel E, Deubener J, Bernard A, Höland M, Muller R, Kappert H, et al. Phenomena and mechanisms of crack propagation in glass-ceramics. J Mech Behav Biomed Mater 2008;1:313-25.

[39] Green DJ. An introduction to the mechanical properties of ceramics. Cambridge solid state science series. New York. Cambridge University Press; 1998. p. 248-60.

[40] Höland W, Schweiger M, Frank M, Rheinberger V. A comparison of the microstructure and properties of the IPS Empress 2 and the IPS Empress glass-ceramics. J Biomed Mater Res 2000;53:297-303.

[41] Quinn GD. Fractography of ceramics and glasses. National Institute of Standards and Technology, Special Publication 960-17, Whashington, U.S. Government Printing Office; 2007. p. 6-1-6-52.

[42] Zhang Y, Lawn BR, Rekow ED, Thompson VP. Effect of sandblasting on the long-term performance of dental ceramics. J Biomed Mater Res B Appl Biomater 2004;71B:381-6.

[43] Darvell BW. Materials science for dentistry. 9th ed. Cambridge. Woodhead publishing Inc.; 2009. p. 451-64.

[44] Menees TS, Lawson NC, Beck PR, Burgess JO. Influence of particle abrasion or hydrofluoric acid etching on lithium disilicate flexural strength. J Prosthet Dent 2014;112:1164-70.

[45] Vidotti HA, Garcia RP, Conti PC, Pereira JR, Valle AL. Influence of low concentration acid treatment on lithium disilicate core/veneer ceramic bond strength. J Clin Exp Dent 2013;5:e157-62.

[46] Xiaoping L, Dongfeng R, Silikas N. Effect of etching time and resin bond on the flexural strength of IPS e.max Press glass ceramic. Dent Mater 2014;30:e330-6.

[47] Addison O, Marquis PM, Fleming GJ. The impact of hydrofluoric acid surface treatments on the performance of a porcelain laminate restorative material. Dent Mater 2007;23:461-8.

[48] Ramakrishnaiah R, Alkheraif AA, Divakar DD, Matinlinna JP, Vallittu PK. The effect of hydrofluoric acid etching duration on the surface micromorphology, roughness, and wettability of dental ceramics. Int J Mol Sci 2016;17:822.

[49] Gresnigt MMM, Özcan M, Carvalho M, Lazari P, Cune MS, Razavi P, et al. Effect of luting agent on the load to failure and accelerated-fatigue resistance of lithium disilicate laminate veneers. Dent Mater 2017;33:1392-401.

[50] Marquis PM. The influence of cements on the mechanical performance of dental ceramics. J Bioceram 1992;5:317-24.

[51] Fleming GJP, Hooi P, Addison O. The influence of resin flexural modulus on the magnitude of ceramic strengthening. Dent Mater 2012;28:769-76.

[52] Braga RR, Cesar PF, Gonzaga CC. Mechanical properties of resin cements with different activation modes. J Oral Rehabil 2002;29:257-62.

[53] Addison O, Marquis PM, Fleming GJ. Quantifying the strength of a resin-coated dental ceramic. J Dent Res 2008;87:542-7.

[54] Cattell MJ, Palumbo RP, Knowles JC, Clarke RL, Samarawickrama DY. The effect of veneering and heat treatment on the flexural strength of Empress 2 ceramics. J Dent 2002;30:161-9.

[55] Faber KT, Evans AG. Crack deflection processes-I.Theory. Acta Metall 1983;31:565-76.

[56] Aurelio IL, Fraga S, Dorneles LS, Bottino MA, May LG. Extended glaze firing improves flexural strength of a glass ceramic. Dent Mater 2015;31:e316-24.

[57] Fischer H, Maier HR, Marx R. Improved reliability of leucite reinforced glass by ion exchange. Dent Mater 2000;16:120-8.

[58] Shillingburg HT, Sather DA, Wilson EL, Jr., Cain JR, Mitchell DL, Blanco LJ, et al. Fundamentals of fixed prosthodontics. 4th ed. Quintessence Publishing; 2012. p. 131-205.

[59] Theocharopoulos A, Chen X, Hill R, Cattell MJ. Reduced wear of enamel with novel fine and nano-scale leucite glass-ceramics. J Dent 2013;41:561-8.

[60] Burke FJ, Lucarotti PS. Ten-year outcome of crowns placed within the General Dental Services in England and Wales. J Dent 2009;37:12-24.

[61] Fradeani M, Redemagni M. An 11-year clinical evaluation of leucite-reinforced glass-ceramic crowns: a retrospective study. Quintessence Int 2002;33:503-10.

LIST OF TABLES

Tables

Table 1

Glass-Ceramic Groups	Starting Temp (°C)	Pressing Temp (°C)	Heating Rate (°C)	Vacuum (%)	holding Time (mins)	Pressing Time (mins)	Pressing Speed (µm/min)	Pressure (Pa)
LG-C/ OLG-C	700	1080	60	N/A	20	*	300	*
IPS e.max® G-C	700	917	60	N/A	25	*	250	*

*parameters automatically regulated by the heat pressing furnace during function.

Table 2

BFS Groups	Glass-Ceramic (G-C) Specimen	Description:
Group 1	LG-C	SGB.
Group 2	LG-C resin-bonded	SGB, etched 5% HF 60s, resin-bonded.
Group 3	LG-C Lapped/ resin-bonded	SGB, tensile surface lapped, etched 5% HF 60s, resin-bonded.
Group 4	OLG-C	SGB.
Group 5	OLG-C resin-bonded	SGB, etched 5% HF 80s, resin-bonded.
Group 6	IPS e.max® G-C	SGB, invex liquid 20 mins, sandblasted 100µm Al_2O_3.
Group 7	IPS e.max® G-C resin-bonded	SGB, invex liquid 20 mins, sandblasted 100µm Al_2O_3, etched 5% HF 20s, resin–bonded.
Group 8	IPS e.max® G-C Lapped/ resin-bonded	SGB, invex liquid 20 mins, sandblasted 100µm Al_2O_3, tensile surface lapped, etched 5% HF 20s, resin–bonded.

LGC= Leucite Glass-Ceramic; OLGC= Optimised leucite Glass-ceramic, SGB= Sandblasted 50µm glass beads

Table 3

Glass-Ceramic Groups	Mean Biaxial Flexural Strength MPa (SD)	Weibull modulus (m)	Confidence Intervals for m (95%)	Characteristic Strength (MPa)	Confidence Intervals for σ_0 (95%)	r^2
Group1 **LG-C**	193.1 (13.9) [a]	17.4[a]	13.8-21.9	198.7 [a]	194.3-203.3	0.89
Group 2 **LG-C** resin-bonded	217.7 (23.0) [b]	11.1 [a,b,c]	8.4-14.8	227.4 [b]	219.7-235.5	0.97
Group 3 **LG-C** lapped/ resin-bonded	273.6 (26.7) [c, d]	11.6 [a,b,c]	8.5-15.7	285.4 [c]	276.0-295.2	0.97
Group 4 **OLG-C**	255.9 (31.0) [c]	9.5 [b,c]	7.1-12.7	269.0 [c,e]	258.3-280.3	0.98
Group 5 **OLG-C** resin-bonded	288.6 (37.4) [d]	8.6 [c]	6.3-11.7	304.7 [d]	291.2-318.9	0.97
Group 6 **IPS e.max® G-C**	258.6 (20.7) [c]	15.1 [a,b,c]	11.6-19.5	267.3 [e]	260.5-274.3	0.95
Group 7 **IPS e.max® G-C** resin-bonded	322.3 (23.4) [e]	16.1 [a,b]	12.1-21.3	332.5 [f]	324.6-340.7	0.97
Group 8 **IPS e.max® G-C** lapped/ resin-bonded	416.4 (52.6) [f]	9.6 [b,c]	7.7-12.1	437.3 [g]	419.9-455.6	0.94

* Significant difference indicated by different superscript letters, m = Weibull modulus; σ_0 = Characteristic strength.

Table 4

Glass-Ceramic Groups	Median SBS (MPa)	Confidence Intervals for Median (25%- 75%)	Mean (SD) SBS (MPa)
Group 1 **LG-C** (60s etch)	14.2 [a]	13.3-15.2	14.5 (1.8)[a]
Group 2 **LG-C** (10s etch)	10.6 [a,b]	7.4-15.5	11.1 (4.4)[b]
Group 3 **IPS e.max® G-C** (20s etch)	10.8 [b]	9.6-14.1	11.6 (2.6)[b]

* Significant differences indicated by different superscript letters in columns.

Table 5

Glass-Ceramic	Function	Before HF etching		After HF etching	
		Mean* X (µm)	Mean* Y (µm)	Mean* X (µm)	Mean* Y (µm)
LG-C	ISO R_a	3.1	3.1	2.6	2.6
IPS e.max® G-C		5.7	5.7	5.1	5.0

(*) represent the mean of 801 profiles.

LIST OF FIGURES

Figure 1, a-h

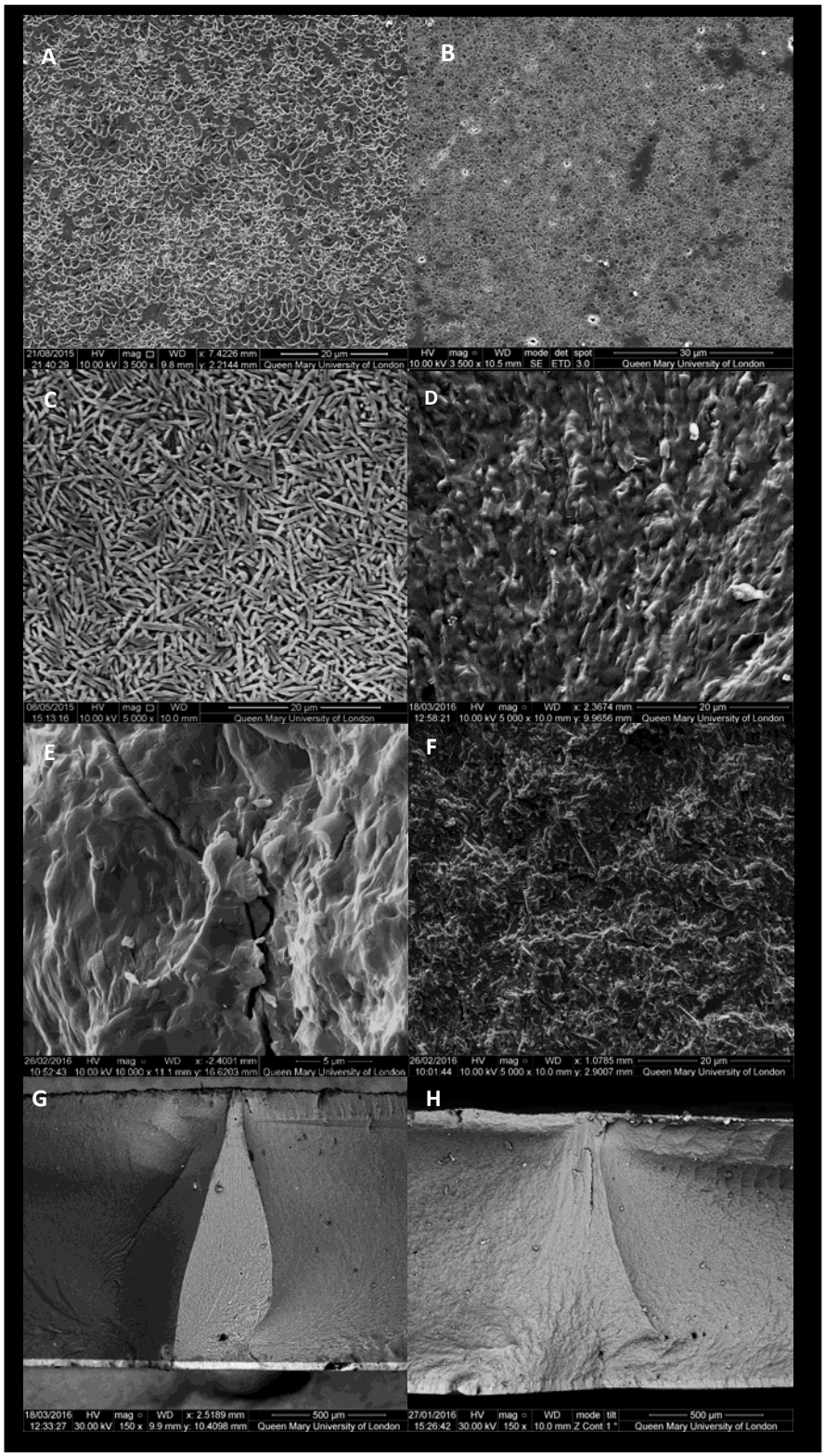

Figure 2, a-d

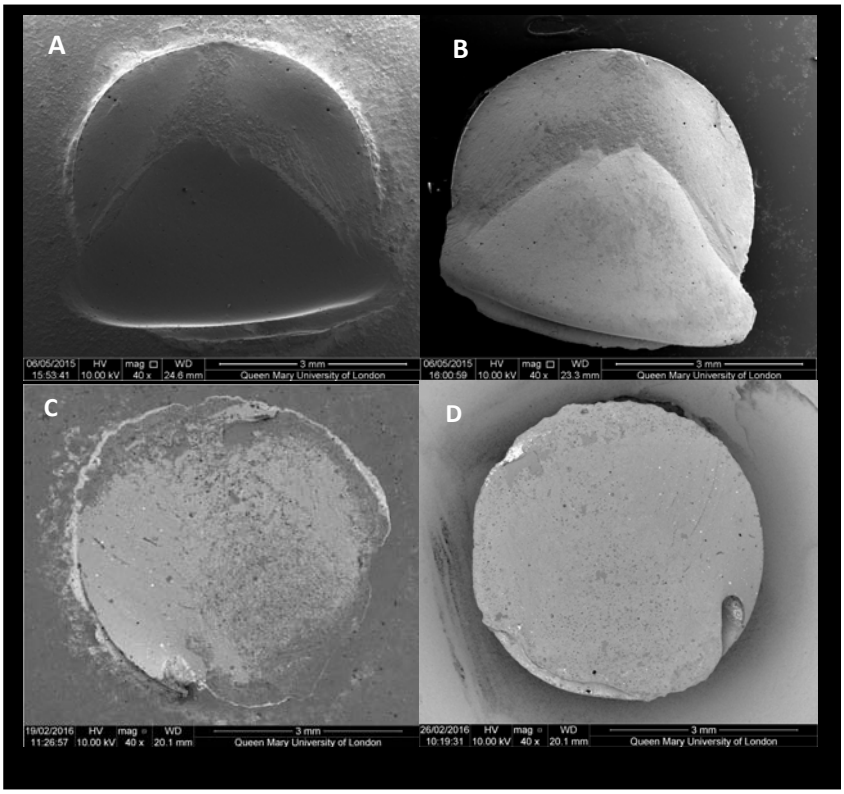
A
B
C
D
06/05/2015 HV mag WD 3 mm
15:53:41 10.00 kV 40 x 24.6 mm Queen Mary University of London
06/05/2015 HV mag WD 3 mm
16:00:59 10.00 kV 40 x 23.3 mm Queen Mary University of London
19/02/2016 HV mag WD 3 mm
11:26:57 10.00 kV 40 x 20.1 mm Queen Mary University of London
26/02/2016 HV mag WD 3 mm
10:19:31 10.00 kV 40 x 20.1 mm Queen Mary University of London

Figure 3a

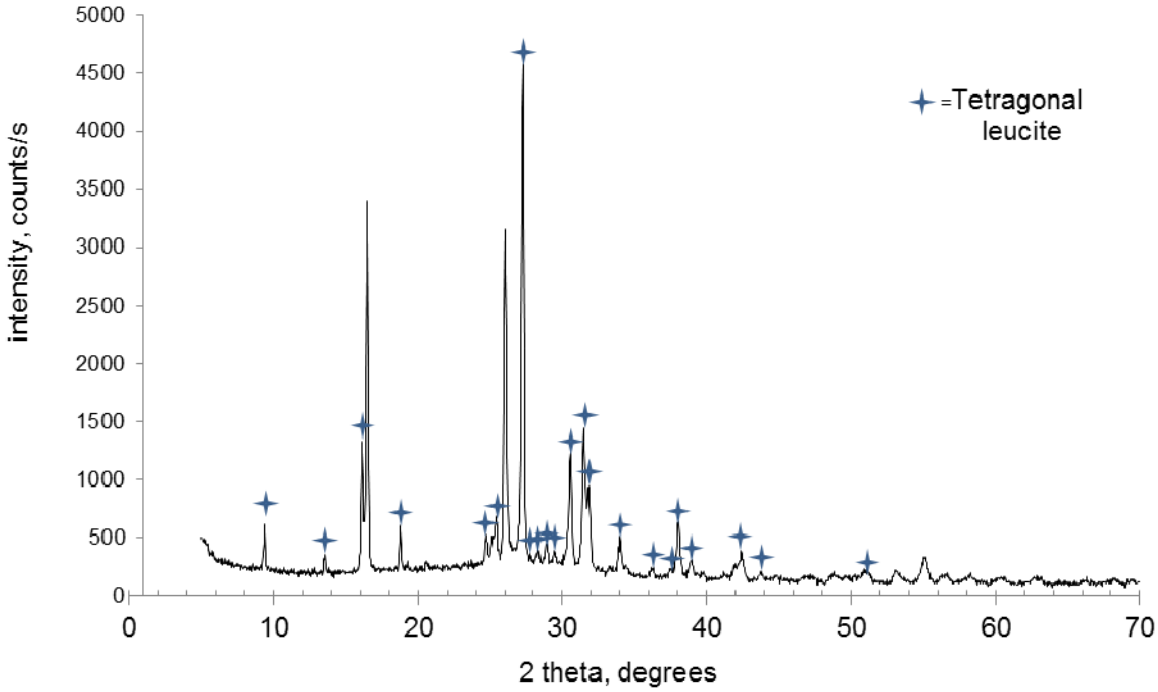
intensity, counts/s
5000
4500
4000
3500
3000
2500
2000
1500
1000
500
0
0
10
20
30
40
50
60
70
2 theta, degrees
=Tetragonal leucite

Figure 3b

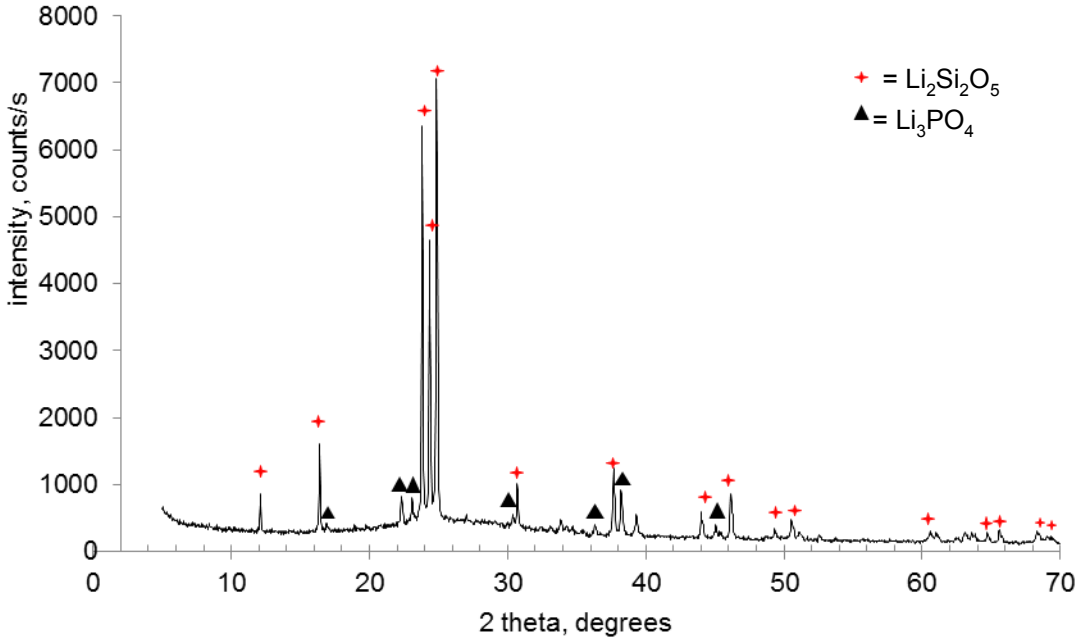
8000
7000
6000
5000
4000
3000
2000
1000
0
intensity, counts/s
0
10
20
30
40
50
60
70
2 theta, degrees
= Li2Si2O5
= Li3PO4

Figure 4a

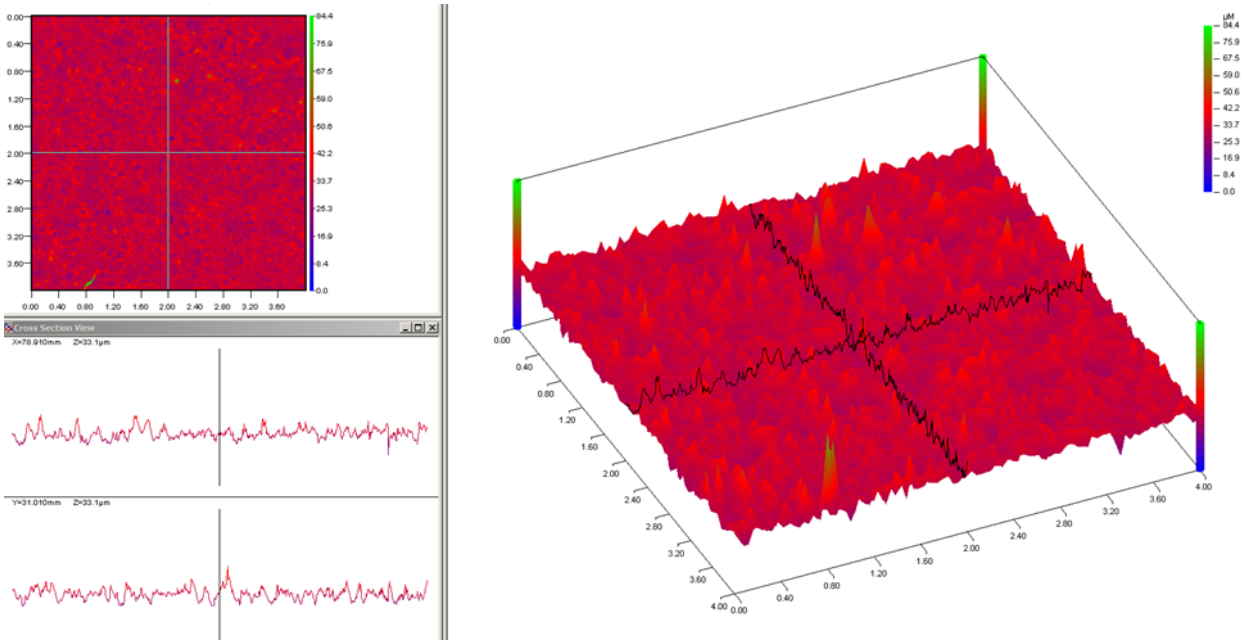
Cross Section View
X=78.910mm Z=33.1µm
Y=31.010mm Z=33.1µm
µM
84.4
75.9
67.5
59.0
50.6
42.2
33.7
25.3
16.9
8.4
0.0
0.00
0.40
0.80
1.20
1.60
2.00
2.40
2.80
3.20
3.60
4.00

Figure 4b